Brazilian Journal
of Chemical
Engineering

ISSN 0104-6632
Printed in Brazil
www.abeq.org.br/bjche

Vol. 29, No. 03, pp. 599 - 611, July - September, 2012

EFFECTIVE TRANSPORT PROPERTIES FOR THE PYRIDINE-GRANULAR ACTIVATED CARBON ADSORPTION SYSTEM

S. A. Baz-Rodríguez[1], R. Ocampo-Pérez[2], J. P. Ruelas-Leyva[1] and C. G. Aguilar-Madera[1*]

[1]División de Ciencias Básicas e Ingenierías, Universidad Autónoma Metropolitana-Iztapalapa,
Apartado Postal 55-534, México D.F. 09340, México.
E-mail: carlos_aguilarmadera@hotmail.com
[2]Centro de Investigación y Estudios de Posgrado, Facultad de Ciencias Químicas,
Universidad Autónoma de San Luis Potosí, Av. Dr. M. Nava No. 6, San Luis Potosí, SLP 78210, México.

(Submitted: July 5, 2011 ; Revised: December 21, 2011 ; Accepted: January 28, 2012)

Abstract - In this work, the kinetics of pyridine adsorption onto granular activated carbon was studied from the point of view of an up-scaling process by using the method of volume averaging. The pore and surface effective diffusivities were estimated by supposing simple microscale geometries (ordered media of cylinders and spheres) and those of images processed from SEM (Scanning Electron Microscopy) micrographs. In addition, as a rough estimate, the point surface diffusivity is reported. The results revealed that the up-scaled diffusional model satisfactorily interpreted the concentration decay curves and the effective diffusivity was found to be an increasing function of the concentration, mainly due to the contribution of surface diffusion. In general, the diffusivity coefficients involved in the adsorption system are related through the expression molecular diffusivity = 22 × point surface diffusivity = 5/2 × pore effective diffusivity = 1/12 × surface effective diffusivity.
Keywords: Pore and surface effective diffusion; Method of volume averaging; Granular activated carbon; Pyridine adsorption.

INTRODUCTION

Pyridine is a colorless and flammable liquid with an unpleasant odor, which is widely used in the manufacturing of fine chemicals (i.e., drugs, vitamins, dyes), agrochemicals, among others (Sabah and Celik, 2002). Due to this, it is commonly found in industrial wastewater, leading to environmental pollution problems. This has motivated several efforts to develop methods to remove pollutants from aqueous solutions such as: biological degradation (Mathur *et al*., 2008; Qiao and Wang, 2010), ozonation (Andreozzi, 1991), adsorption (Lataye *et al*., 2008; Ocampo-Pérez *et al*., 2010) and others.

In adsorption systems, granular activated carbon (GAC) is one of the most efficient adsorbents used for removing organic compounds from aqueous solutions (Liu *et al*., 2009). GAC has been considered in the U.S. by the EPA (Environmental Protection Agency) to be one of the best available technologies for controlling several aromatic pollutants (volatile organic compounds, phenols, pesticides and herbicides) (Zhang and Wang, 2009) due to its chemical and morphological properties (Moreno-Castilla *et al*., 1995). Moreover, it has been reported that GAC can efficiently remove pyridine from aqueous solution (Mohan *et al.*, 2004; Lataye *et al*., 2008).

The global adsorption rate on porous materials like GAC involves three consecutive steps: external mass transport, intraparticle diffusion and adsorption on active sites of the solid matrix. The intraparticle diffusion can be due to pore volume diffusion,

*To whom correspondence should be addressed

surface diffusion, or a combination of both mechanisms (Leyva-Ramos and Geankoplis, 1994; Ocampo-Pérez *et al*., 2010). Pore volume diffusion refers to the movement of the adsorbate due to concentration gradients in the fluid-phase (i.e., molecular mechanisms), but affected by the geometry of the porous matrix. For diluted solutions, the pore volume diffusion depends only on the molecular diffusivity and the spatial distribution of phases at the microscale. The latter concept defines the geometrical properties of the porous medium such as the porosity and the tortuosity. Surface diffusion refers to the movement of the adsorbate through the solid surface and is also influenced by the distribution of phases; the main driving force is the surface concentration gradient. It has been found that surface diffusion depends on the surface concentration and the sorptive affinity between the molecules of adsorbate and adsorbent (Suzuki and Fujii, 1982; Furuya *et al*., 1996).

In many systems presenting a hierarchy of scales, like GAC, one of the main challenges is the theoretical description on a convenient scale of observation. Thus, for design and modeling macroscale average quantities are enough, but in order to take into account the physics at lower size scales an up-scaling method is required. One standard procedure is the method of volume averaging (Whitaker, 1999) which has been used in many types of transport problems. For instance, Ochoa-Tapia *et al*. (1993) carried out the theoretical up-scaling of the diffusive and adsorptive transport of solute considering a linear isotherm in a homogeneous two-phase porous medium and reported the associated closure problems for prediction of the effective properties. Subsequently, Guelli U. de Souza *et al*. (2007) incorporated the effect of bulk and surface reactions in their study of the dyeing of packed cotton threads and also reported the associated closure problems for prediction of the effective properties. Nonetheless, the influence of reactive conditions on effective properties like the effective diffusivity is unclear and some efforts have been devoted in the literature to gaining insight into this issue (Borges da Silva *et al*., 2007; Valdés-Parada and Alvarez-Ramírez, 2010; Valdés-Parada *et al*., 2011).

The closure problems arising theoretically in the method of volume averaging must be solved in representative domains of the microstructure in order to predict the effective transport properties. Thus, simple geometries have commonly been used (Chang, 1983, Whitaker, 1999). Even some more complicated domains from real material images have been employed (Lux *et al*., 2006).

In this work, the problem of adsorption of pyridine onto GAC was studied from the point of view of an up-scaling process and the corresponding effective transport properties were determined. In order to model mass transport, we retook the theoretical up-scaling process carried out by Ochoa-Tapia *et al*. (1993) for the phenomenon on the microscale via the volume averaging method. Thus, governing equations on the macroscale are obtained that are expressed in terms of effective properties. These equations were used to interpret experimental data and to predict the pore and surface effective diffusivities. To this end, the microstructure was assumed to have simple geometries (ordered media of cylinders and spheres) or were obtained from images processed from SEM (Scanning Electron Microscopy) micrographs. Furthermore, as a rough estimate, the point surface diffusivity is reported.

UP-SCALING OF MASS TRANSPORT

The system under study is presented in Figure 1. This consists of a fluid phase in which the adsorbate is diluted and of particles of the porous adsorbent media. In order to clearly identify each homogenous portion of the system (i.e., a portion with position-independent effective properties), two different regions were defined: the η-region represents the homogenous fluid outside the particles of adsorbent; such particles are named the ω-region. Since the ω-region is composed of two phases (the solid matrix and the fluid within the pores), it is necessary to focus first on the derivation of the governing equation for mass transport in this region.

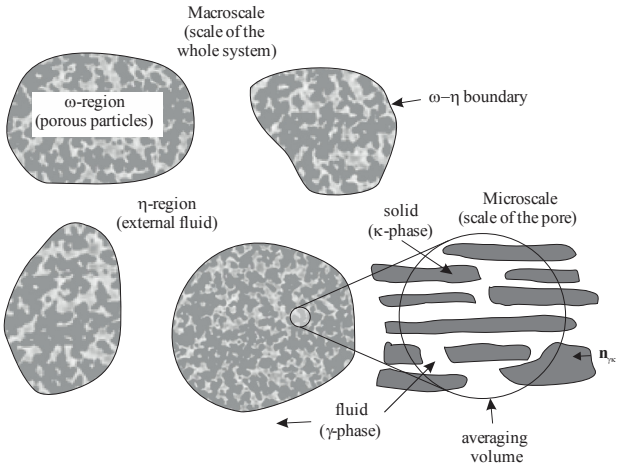

Figure 1: Sketch of the length-scales of the system, phases and volume averaging.

Mass Transport Description on the Microscale in the Porous Particle

The up-scaling process begins by defining the mass balance for the adsorbate on the pore-scale (microscale). A single fluid phase (γ-phase) is considered that completely saturates the interstices of the solid matrix (κ-phase), comprising the porous region (see Figure 1). In this type of system, it is appropriate to neglect the mass transport by convection within the pores as long as the associated Reynolds number is less than 1, which implies that mass transport mainly occurs by diffusive processes. Thus, the mass balance of pyridine (identified by the subscript A) inside the pores is given by:

In the γ-phase

$$\underbrace{\frac{\partial c_{A\gamma}}{\partial t}}_{\text{acumulation}} = \underbrace{\nabla\cdot\left(D_{A\gamma}\nabla c_{A\gamma}\right)}_{\text{diffusion}} \quad (1)$$

which is valid for dilute solutions. In the above equation $c_{A\gamma}$ represents the adsorbate concentration on the microscale, $D_{A\gamma}$ is the molecular diffusivity and ∇ is the spatial differential operator. The surface mass transport at the fluid-solid interface (γ-κ) is expressed as (Slattery, 1990, section 5.2.1),

At the γ-κ interface

$$\underbrace{\frac{\partial c_{As}}{\partial t}}_{\substack{\text{surface}\\ \text{accumulation}}} = \underbrace{-\mathbf{n}_{\gamma\kappa}\cdot\left(D_{A\gamma}\nabla c_{A\gamma}\right)}_{\substack{\text{normal mass flux from}\\ \text{(or to) the fluid}}} + \underbrace{\nabla_s\cdot\left(D_{As}\nabla_s c_{As}\right)}_{\text{surface diffusion}} \quad (2)$$

where c_{As} is the surface adsorbate concentration at the $\gamma-\kappa$ interface, $\mathbf{n}_{\gamma\kappa}$ is the unit normal vector pointing from the fluid phase to the solid phase, D_{As} represents the point surface diffusivity of the adsorbate and, in this case, ∇_s is the surface differential operator [see Eq. (1.11) in the work of Ochoa-Tapia *et al*. (1993) for its definition]. In Eq. (2) it has been explicitly pointed out that the surface mass balance for the adsorbed pyridine encompasses accumulation, mass flux from or to the pore bulk and transport by a diffusive mechanism. As a matter of fact, the term $-\mathbf{n}_{\gamma\kappa}\cdot\left(D_{A\gamma}\nabla c_{A\gamma}\right)$ allows quantifying the mass of pyridine adsorbed or desorbed at a certain position of the fluid-solid interface.

The problem of mass transport on the microscale is completed by setting the initial conditions for the pore and surface concentrations and the boundary conditions applying at the limits of the system. It is worth pointing out that the different concentrations handled in Eqs. (1) and (2) differ in the units, so $c_{A\gamma}$ has units of mass/volume and c_{As} of mass/area. In addition, $D_{A\gamma}$ and D_{As} are physical properties related to the microscale and it is important to clearly distinguish from the effective transport properties involved in the upscaled models (explained later), which are related to the volume averaging scale.

Macroscale Description within the Adsorbent Medium

Effective Medium Equation

In principle, it is possible to describe completely the pyridine transport by numerically solving the microscale governing equations. However, it is a highly demanding computational task and possibly unnecessary, given that, for practical purposes, it is enough to describe the mass transport by using up-scaled models (effective medium equations) which are expressed in terms of average variables and effective transport properties. Generally, such up-scaled models are obtained by: 1) postulating the form of the equations, 2) applying some up-scaling method to the microscale governing equations. In this work, the theoretical results of Ochoa-Tapia *et al*. (1993) are used in which the method of volume averaging was applied for the up-scaling process. These researchers derived the effective medium equation for solute mass transport in the porous particle (ω-region):

$$\underbrace{\varepsilon_\gamma\left(1+\frac{a_v K_{eq}}{\varepsilon_\gamma}\right)\frac{\partial\left\langle c_{A\gamma}\right\rangle_\omega^\gamma}{\partial t}}_{\text{accumulation}} = \underbrace{\nabla\cdot\left(\varepsilon_\gamma\mathbf{D}_{eff}\cdot\nabla\left\langle c_{A\gamma}\right\rangle_\omega^\gamma\right)}_{\text{diffusion}} \quad (3)$$

where ε_γ is the porosity, a_v is the interfacial area per unit volume, $\mathbf{D}_{eff}$ is the effective diffusivity tensor and $\left\langle c_{A\gamma}\right\rangle_\omega^\gamma$ is the intrinsic average concentration in the porous particle, defined as,

$$\left\langle c_{A\gamma}\right\rangle_\omega^\gamma = \frac{1}{V_\gamma}\int_{V_\gamma} c_{A\gamma}\,dV \quad (4)$$

Here V_γ represents the portion of the averaging volume occupied by the fluid-phase (see Figure 1). Notice that the form of Eq. (3) is similar to the microscale balance equation, Eq. (1), but with the term for accumulation modified by the adsorption equilibrium and the porosity. In addition, in Eq. (3) K_{eq} is the adsorption equilibrium constant, assuming the following linear constitutive expression:

$$c_{As} = K_{eq} c_{A\gamma} \tag{5}$$

It must be mentioned that expression (5) is a strong assumption since it has been demonstrated that the pyridine-GAC adsorption system obeys a Prausnitz-Radke isothermal model (Ocampo-Pérez *et al*., 2010). As a matter of fact, one can think of the coefficient K_{eq} as being the derivative of the adsorption isotherm at a given value of $c_{A\gamma}$ as is suggested in Figure 2. With this in mind, a decreasing dependency of K_{eq} with concentration is expected, which is corroborated later in the work.

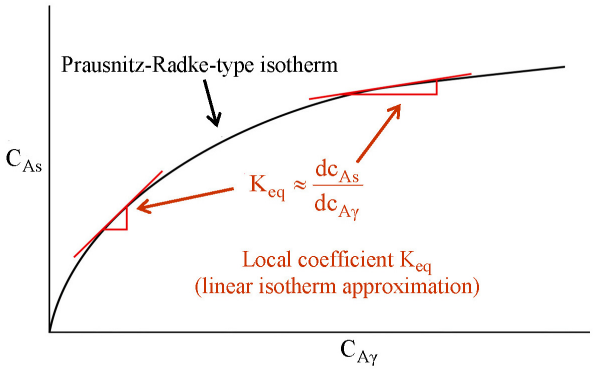

Figure 2: Interpretation of the equilibrium constant K_{eq}.

Eq. (3) is valid at every point within the porous bulk, shown in Figure 1 and its validity is reduced as we approach to the ω–η boundary. Strictly, in order to use Eq. (3) close to the particle porous-fluid boundary, more detailed work about the jump boundary condition that applies at such boundary is required (Valdés-Parada *et al*., 2009); however, the development and implementation of this type of boundary conditions are beyond the scope of this paper. In addition, it should be stressed that, in obtaining Eq. (3), one of the main assumptions is that the adsorption equilibrium follows a linear behavior.

Closure

Eq. (3) is in closed form since it does not contain unknown (or empirical) parameters and it is explicitly related to the geometrical and physical microscale properties. Thus, the effective diffusivity tensor is given by (Ochoa-Tapia *et al*., 1993):

$$\varepsilon_\gamma \mathbf{D}_{eff} = \varepsilon_\gamma D_{A\gamma}\left(\mathbf{I} + \frac{1}{V_\gamma}\int_{A_{\gamma\kappa}} \mathbf{n}_{\gamma\kappa}\Omega\mathbf{f}dA\right) + a_v K_{eq} D_{As}\mathbf{I} \tag{6}$$

where $\mathbf{I}$ is the identity tensor, $A_{\gamma\kappa}$ represents the geometric place of the fluid-solid interface, $\mathbf{f}$ is the so-called closure vector and Ω is a function defined as,

$$\Omega = 1 + \frac{2HK_{eq}D_{As}}{D_{A\gamma}} \tag{7}$$

where H represents the mean curvature radius of the $\gamma-\kappa$ interface (Slattery, 1990, section A5.3). In cases without adsorption, $K_{eq}, D_{As} = 0$ and the expression valid for passive diffusion is given by (Ryan *et al*., 1981):

$$\mathbf{D}_p = D_{A\gamma}\left(\mathbf{I} + \frac{1}{V_\gamma}\int_{A_{\gamma\kappa}} \mathbf{n}_{\gamma\kappa}\mathbf{f}dA\right) \tag{8}$$

To differentiate from the effective diffusivity ($\mathbf{D}_{eff}$), $\mathbf{D}_p$ is used as the pore effective diffusivity tensor which is only a function of the molecular diffusivity and of the microstructure (quantified through the integral) commonly associated with the tortuosity. Several works have been addressed to obtain theoretical and experimental values of $\mathbf{D}_p$ for various porous materials (Currie, 1960; Ryan *et al*., 1981; among others).

The closure variable $\mathbf{f}$ satisfies the following steady boundary value problem (closure problem).

In the γ-phase $\quad \nabla^2\mathbf{f} = \mathbf{b}$ (9)

At $A_{\gamma\kappa}$ $\quad \mathbf{n}_{\gamma\kappa}\cdot\left(D_{A\gamma}\nabla\mathbf{f}\right) = \mathbf{g} - \mathbf{n}_{\gamma\kappa}D_{A\gamma}$ (10)

Periodicity conditions

$$\mathbf{f}(\mathbf{r}) = \mathbf{f}(\mathbf{r} + l_i),\ i = 1,2,3 \tag{11}$$

where

$$\mathbf{b} = \frac{1}{V_\gamma}\int_{V_\gamma} \nabla^2 \mathbf{f} dV \tag{12}$$

$$\mathbf{g} = K_{eq} D_{As}\left(\nabla_s \cdot \nabla_s \mathbf{f}\right) - 2\mathbf{n}_{\gamma\kappa} H K_{eq} D_{As} \tag{13}$$

The closure problem is solved in representative zones of the homogeneous porous medium namely unit cell. The periodicity conditions are applied at the external boundaries of the unit cell. The formal derivation of such a closure problem implies the assumptions of several length-scale and time restrictions that must be considered during the application step. The presentation and discussion of these restrictions is vast and is beyond the scope of this work. Thus, for a detailed discussion of the validity and theoretical development of the closure problem we refer the reader to the work of Ochoa-Tapia *et al*. (1993).

Note that the definition of the effective diffusivity, Eq. (6), cannot be divided in two contributions for pore and surface diffusion because the variables $\mathbf{f}$ and Ω depend on the values of K_{eq} and D_{As}. Moreover, following the developments of Ochoa-Tapia *et al*. (1993) it is possible to carry out the decomposition [see Eq. (4.43) therein],

$$\mathbf{D}_{eff} = \mathbf{D}_p + \mathbf{D}_s \tag{14}$$

In this case, the closure problem for prediction of $\mathbf{D}_p$ is obtained by setting $\mathbf{b}$ and $\mathbf{g}$ equal to zero in Eqs. (9)-(11). In Eq. (14) $\mathbf{D}_s$ is the surface effective diffusivity, which is a function of the physical properties $(K_{eq}, D_{As}, D_{A\gamma})$ and the geometrical parameters $(a_v, \varepsilon_\gamma)$ of the microscale. In this way, knowing the individuals values for $\mathbf{D}_{eff}$ and $\mathbf{D}_p$, the corresponding one for $\mathbf{D}_s$ can be calculated. Using Eq. (13), the scaled model (3) can be rewritten as,

$$\underbrace{\varepsilon_\gamma\left(1+\frac{a_v K_{eq}}{\varepsilon_\gamma}\right)\frac{\partial\left\langle c_{A\gamma}\right\rangle_\omega^\gamma}{\partial t}}_{\text{accumulation}} = \nabla\cdot\left(\underbrace{\varepsilon_\gamma \mathbf{D}_p\cdot\nabla\left\langle c_{A\gamma}\right\rangle_\omega^\gamma}_{\text{pore effective diffusion}} + \underbrace{\varepsilon_\gamma \mathbf{D}_s\cdot\nabla\left\langle c_{A\gamma}\right\rangle_\omega^\gamma}_{\text{surface effective diffusion}}\right) \tag{15}$$

This equation presents a form similar to those models usually used for experimentally determining the values of the surface effective diffusion coefficient (Ocampo-Pérez *et al*., 2010), but the substantial difference lies in the available clear physical meaning of the coefficients involved.

Solution of the Closure Problem

The domain in which the closure problem is solved must contain enough information about geometrical features of the porous material in order to accurately capture the distribution of phases on the microscale. With this idea in mind, SEM images of the GAC, filtered with an image processing software, are one of the best options. Nevertheless, the solution of the closure problem on simplified geometries like those shown in Figure 3 (geometrical models 1 and 2) is generally enough to obtain acceptable predictions of the effective properties (Ryan *et al*., 1981; Nozad *et al*., 1985) and to elucidate the effect of variables (such as the porosity and the equilibrium constant). Thus, in this work, the three geometrical models shown in Figure 3 are used and the results are compared.

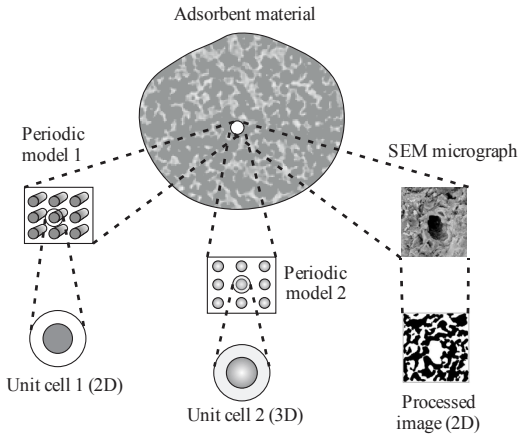

Figure 3: Geometric models of unitary cells to represent the microstructure of the adsorbet material.

Ochoa-Tapia *et al*. (1993) analytically solved the closure problem in 2D and 3D Chang cells (units cells 1 and 2 shown in Figure 3) (Chang, 1983). Using the 2D cell, the longitudinal component of the effective diffusivity is given by:

$$\frac{\varepsilon_\gamma D_{eff}}{D_{A\gamma}} = \frac{\varepsilon_\gamma\left[\left(2-\varepsilon_\gamma\right)+\varepsilon_\gamma\Lambda - \left(1-\Lambda\right)^2\left(1-\varepsilon_\gamma\right)\right]}{\left(2-\varepsilon_\gamma\right)+\varepsilon_\gamma\Lambda} + 2\left(1-\varepsilon_\gamma\right)\Lambda \tag{16}$$

where

$$\Lambda = \frac{K_{eq} D_{As} a_v}{2\left(1-\varepsilon_\gamma\right) D_{A\gamma}} \tag{17}$$

while for the 3D cell:

$$\frac{\varepsilon_\gamma D_{eff}}{D_{A\gamma}} = \frac{\varepsilon_\gamma\left[\begin{array}{l}\left(3-\varepsilon_\gamma\right)+2\varepsilon_\gamma\Lambda- \\ \left(1-2\Lambda\right)^2\left(1-\varepsilon_\gamma\right)\end{array}\right]}{\left(3-\varepsilon_\gamma\right)+2\varepsilon_\gamma\Lambda} + 3\left(1-\varepsilon_\gamma\right)\Lambda \tag{18}$$

with

$$\Lambda = \frac{K_{eq} D_{As} a_v}{3\left(1-\varepsilon_\gamma\right) D_{A\gamma}} \tag{19}$$

For the pyridine-GAC adsorption system, geometrical and physical properties (like the interfacial area and the molecular diffusivity) are available in the literature (Ocampo-Pérez *et al*., 2010). Nevertheless, to the best of our knowledge, there are no reported values for the point coefficient D_{As}. In this regard, Eqs. (16) and (18) allow us to move in either of two directions:

- All the microscale parameters ($D_{A\gamma}$, K_{eq}, D_{As}, distribution of phases) being available, we are able to predict all the macroscale ones ($\mathbf{D}_{eff}$, ε_γ, a_v) or,
- From the known values of all the macroscale and microscale parameters except one of the physical properties, we are in a position to predict the remaining one.

Thus, it is possible from comparisons with experimental data to obtain the effective diffusivity and, with the known values of porosity, molecular diffusivity, equilibrium constant and interfacial area, and assuming the microstructure, we can infer the value of D_{As}.

Macroscale Model for the Entire System

The intraparticle mass transport governed by Eq. (3) is coupled with the corresponding mass balance equation in the fluid región (η-region shown in Figure 1) given by:

$$V\frac{\partial\left\langle c_{A\gamma}\right\rangle_\eta^\gamma}{\partial t} = -mSk_L\left(\left\langle c_{A\gamma}\right\rangle_\eta^\gamma - \left\langle c_{A\gamma}\right\rangle_\omega^\gamma\Big|_{\mathbf{x}_{\omega\eta}}\right) \tag{20}$$

where V is the volume of the external fluid; $\left\langle c_{A\gamma}\right\rangle_\eta^\gamma$ is the intrinsic average concentration of adsorbate in the η-region, defined in a similar form to Eq. (4); m is the mass of adsorbent in the system; S represents the contact area per mass of adsorbent between the GAC and the external fluid (ω–η boundary sketched in Figure 1); k_L is the mass transfer coefficient for the external fluid, and $\mathbf{x}_{\omega\eta}$ represents the vector locating the ω–η boundary. In addition, it should be stressed that Eq. (20) assumes a perfectly mixed external fluid.

The governing equations for each homogeneous region are matched with the following boundary condition,

$$\begin{aligned}&\mathbf{n}_{\omega\eta}\cdot\left[\varepsilon_\gamma\left(\mathbf{D}_p+\mathbf{D}_s\right)\cdot\nabla\left\langle c_{A\gamma}\right\rangle_\omega^\gamma\right] = \\ &\mathbf{n}_{\omega\eta}\cdot\left(D_{A\gamma}\nabla\left\langle c_{A\gamma}\right\rangle_\eta^\gamma\right),\ \text{at } \mathbf{x}_{\omega\eta}\end{aligned} \tag{21}$$

where $\mathbf{n}_{\omega\eta}$ is the unit normal vector pointing from the ω- to the η-region. Eq. (21) implies continuity for the mass flux through the ω–η boundary and, therefore, surface accumulative effects (excess quantities) have been discarded. A study focused on measuring excess quantities is beyond the scope of this work, and the problematic is treated in the following way. For systems where resistance to mass transfer is greater in the external fluid, the right hand of Eq. (21) can be simplified according to the expression (Leyva-Ramos and Geankoplis, 1994; Ocampo-Pérez *et al*., 2010),

$$\begin{aligned}&\mathbf{n}_{\omega\eta}\cdot\left(D_{A\gamma}\nabla\left\langle c_{A\gamma}\right\rangle_\eta^\gamma\right) = \\ &k_L\left(\left\langle c_{A\gamma}\right\rangle_\eta^\gamma - \left\langle c_{A\gamma}\right\rangle_\omega^\gamma\right),\ \text{at } \mathbf{x}_{\omega\eta}\end{aligned} \tag{22}$$

Note that Eqs. (15) and (21) can be applied to whatever coordinate system. Thus, assuming spherical porous particles, the model can be rewritten as:

$$\begin{aligned}&\varepsilon_\gamma\left(1+\frac{a_v K_{eq}}{\varepsilon_\gamma}\right)\frac{\partial\left\langle c_{A\gamma}\right\rangle_\omega^\gamma}{\partial t} = \\ &\frac{1}{r^2}\frac{\partial}{\partial r}\left[r^2\varepsilon_\gamma\left(D_p+D_s\right)\frac{\partial\left\langle c_{A\gamma}\right\rangle_\omega^\gamma}{\partial r}\right],\ \text{in the } \omega\text{-region}\end{aligned} \tag{23}$$

$$\varepsilon_\gamma \left(D_p + D_s \right) \frac{\partial \left\langle c_{A\gamma} \right\rangle_\omega^\gamma}{\partial r} = k_L \left(\left\langle c_{A\gamma} \right\rangle_\eta^\gamma - \left\langle c_{A\gamma} \right\rangle_\omega^\gamma \right), \quad \text{at } r = R_p \tag{24}$$

$$V \frac{\partial \left\langle c_{A\gamma} \right\rangle_\eta^\gamma}{\partial t} = -mSk_L \left(\left\langle c_{A\gamma} \right\rangle_\eta^\gamma - \left\langle c_{A\gamma} \right\rangle_\omega^\gamma \Big|_{r=R_p} \right), \quad \text{in the } \eta\text{-region} \tag{25}$$

where R_p is the particle radius. In these equations gradients in the angular directions have been discarded, assuming that significant changes take place only in the radial direction. The model is complemented by the symmetry condition

$$\frac{\partial \left\langle c_{A\gamma} \right\rangle_\omega^\gamma}{\partial r} = 0, \text{ at } r = 0 \tag{26}$$

and the initial conditions

$$\left\langle c_{A\gamma} \right\rangle_\omega^\gamma = 0, \text{ at } t = 0 \tag{27}$$

$$\left\langle c_{A\gamma} \right\rangle_\eta^\gamma = C_{A0}, \text{ at } t = 0 \tag{28}$$

where C_{A0} is the initial concentration of adsorbate in the external fluid.

METHODOLOGY

Experimental Procedure

Adsorbent

The granular activated carbon was manufactured from a bituminous carbon by Calgon, Inc. (Pittsburgh, PA) and commercially available as F-400. The GAC was sieved to an average particle diameter of 1.02 mm, washed several times with deionized water, dried at 110°C for 24 h and stored under isolated conditions. The surface area, pore volume and average pore diameter of GAC were determined by the N_2-BET method using a physisorption equipment (Micromeritics Model ASAP 2010), with S_V = 925 m^2/g, V_p = 0.534 cm^3/g, and d_p = 2.2 nm, respectively. The solid density was ρ_s = 2.320 g/cm^3 determined by the helium displacement method using a helium pycnometer (Micromeritics Model Accupic 1330). The particle density and void fraction were ρ_p = 1.036 g/cm^3 and ε_p = 0.554, respectively. The molecular diffusivity of pyridine in aqueous solution at 25 °C is 7.7×10^{-6} cm^2/s (Ocampo-Pérez *et al*., 2010).

Adsorption Equilibrium Data

An Erlenmeyer flask of 500 mL was used as a batch adsorber for obtaining the experimental adsorption equilibrium data. A Nylon mesh bag with a known load of GAC was introduced into the flask and then the pyridine solution was added. The adsorption process was isothermal and continuously stirred. The experimental adsorption equilibrium data for pyridine on GAC were obtained as follows. A Nylon mesh bag with 1 g of GAC and 480 mL of a pyridine solution, with a known initial concentration at pH=10, were added to the batch adsorber. The adsorption equilibrium of pyridine on CAG at different pH and temperature values was previously studied by Ocampo-Perez *et al*. (2010) and they showed that, at pH 10, GAC presents the highest adsorption capacity to remove pyridine from aqueous solution. Therefore, this pH was chosen to study the pyridine adsorption rate on GAC.

The initial pyridine concentration was varied from 20 to 1000 mg/L. The pyridine solution was maintained in contact with the GAC particles until equilibrium was reached. The solution pH was measured periodically and kept constant by adding 0.01 and 0.1 M solutions of HCl and NaOH, as appropriate. After reaching equilibrium, the pyridine concentration in the solution was determined spectrophotometrically and the mass of pyridine adsorbed at equilibrium was calculated by making a mass balance of pyridine. In previous runs without GAC, it was demonstrated that pyridine did not adsorb on the Nylon bag.

Determination of Pyridine Concentration in Water Solution

The pyridine concentration in aqueous solution was determined by UV-Visible spectroscopy. The absorbance of a pyridine solution was measured using a Shimadzu model UV-160 spectrophotometer at a wavelength of 249.5 nm. Thus, the pyridine concentration of a sample was estimated with a calibration curve (absorbance vs. concentration) prepared with five standard pyridine solutions in the concentration range of 10-50 mg/L.

Method to Obtain the Rate of Adsorption Data

A rotating basket batch adsorber was used to obtain the concentration profiles for pyridine

adsorption on GAC. The adsorber was composed of a 1 L three-neck reaction flask and an impeller with its blades replaced with stainless steel baskets. A pyridine solution was poured into the adsorber and the GAC particles were placed in the stainless steel mesh baskets, which were attached to a shaft connected to a variable speed motor. The adsorber was partially immersed in a constant temperature water bath.

A pH=10 solution (800-980 mL) was prepared by appropriately mixing 0.01N HCl and NaOH solutions and added to the adsorber. The baskets containing GAC (1-5 g) were subject to several rotating speed conditions (100, 150, 200 rpm) according to the experiment. The pH of the solution was controlled by appropriately adding 0.01 and 0.1N NaOH solutions. The solution and GAC were left in contact until the temperature and pH remained constant. Subsequently, the stirrer was turned off and an aliquot of a solution of known concentration of pyridine at pH = 10 was expeditiously poured into the adsorber solution to obtain the desired initial concentration. After the addition, the total volume of the solution was 1 L. Right away, the impeller motor and the timer were turned on. The solution pH was monitored with a pH-meter and adjusted as mentioned above. The total volume of NaOH solution added was always less than 2 mL and this volume represented 0.1% of the total volume. The solution was periodically sampled (5 mL) and analyzed to determine the pyridine concentration. Sampling times were 0, 1, 3, 5, 10, 15, 20, 25, 30, 40, 50, 60, 90, 120, 150, and 180 min. The total volume of the adsorber solution (1 L) was kept constant by adding 5 mL of a make-up solution immediately after sampling. The concentration of the make-up solution was the average of the initial concentration and the final concentration at equilibrium. The purpose of this addition was to replace the mass of pyridine withdrawn in the sample. Errors due to sampling and adding make-up solution were calculated by performing a mass balance and were always less than 2 % in all experiments.

Image Processing and Numerical Solution

The morphology of GAC was examined by means of a scanning electron microscope (Leica-Cambridge, model S420-I) using a magnification factor of 2400x. The images were processed by using the Image Processing Toolbox included in the commercial software Matlab. The procedure was as follows. Firstly, the contrast between dark and light zones was improved by translation to grayscale [from 0 (black) to 255 (white)]. Since dark zones visually indicate profundity, it was assumed that these represent the portion occupied by pores, whereas light zones are related to the solid matrix (GAC). With this idea in mind, the grayscale value of each pixel was tracked (from the black color) and accumulated to give the volumetric fraction ε_γ of the darker pixels. Secondly, all the pixels with a value equal or less than a threshold value were converted to white (space occupied by pores), whereas pixels with higher values to black (solid matrix). Finally, in order to enhance the definition of the contours, filters were applied. This procedure allows us to obtain a final binary image in which the ratio between white and total number of pixels equals the porosity of the GAC. Indeed, the processed images from the SEM micrographs provided the domains in which the closure problem was solved. For this purpose, the finite element solver COMSOL Multiphysics® 3.5a was used to obtain the field solution of the closure problem associated with the effective tensor $\mathbf{D}_p$.

The effective diffusivity (D_{eff}) was determined by comparison between experimental and numerical dynamic profiles of the pyridine concentration in the solution. The numerical profiles were obtained by solving the diffusional model given in Equations (23)-(28) using COMSOL Multiphysics® 3.5a. The values reported in this work are those calculated when the experimental and numerical profiles matched within an average relative error of 0.05. The average relative error is defined as follows:

$$\text{error} = \frac{1}{n}\sum_{i=1}^{n}\left|\frac{\left\langle c_{A\gamma}\right\rangle^{\gamma}_{\eta,exp} - \left\langle c_{A\gamma}\right\rangle^{\gamma}_{\eta,num}}{\left\langle c_{A\gamma}\right\rangle^{\gamma}_{\eta,exp}}\right| \tag{29}$$

with n being the total number of experimental data for each experiment. Knowing the values of D_{eff} and D_p, the surface effective diffusivity was then calculated using Eq. (14). Moreover, D_s and D_{As} were calculated from the solution of the closure problems [Eqs. (16)-(19)] in cylindrical and spherical Chang unit cells.

RESULTS AND DISCUSSION

As a first step to predict the effective properties of the pyridine-GAC adsorption system, the diffusional model given by Eqs. (23)-(28) was solved and fitted with the set of experimental data. The dynamical results are depicted in Figure 4, in which

$\Phi = \left\langle c_{A\gamma} \right\rangle_{\eta}^{\gamma} \Big/ C_{A0}$ means the non-dimensional concentration in the solution. For all the cases shown, the diffusional model interprets the experimental data reasonably well, with the following average relative errors: 0.05, 0.032, 0.0084, 0.014, and 0.0084 for $\left\langle c_{A\gamma} \right\rangle_{\eta,eq}^{\gamma}$ = 41.4, 66.3, 80.8, 99.9 and 129.4 mg/L, respectively. As expected, the higher the equilibrium concentration, the more time necessary to reach equilibrium, though in practical terms 180 min were enough in each experiment.

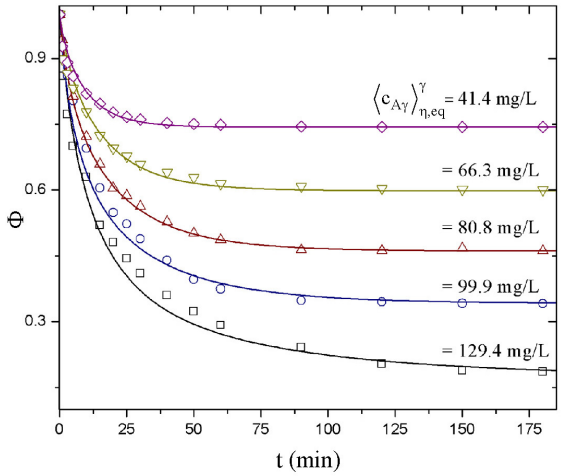

Figure 4: Concentration decay curves for pyridine adsorption on GAC. Lines represent up-scaled diffusional model predictions.

The fitted diffusional model provides the effective transport properties. The effective diffusivity vs. the equilibrium pyridine concentration in the solution is presented in Figure 5, where D_{eff} is found to be an increasing function of the concentration. In this case, as stated in Eq. (14), the effective diffusivity encompasses two different contributions: the pore and the surface effective diffusivities. Since the first one is independent of concentration (i.e., only depends on the microstructure and the molecular diffusivity), the dependency of the effective diffusivity shown in Figure 5 is due to the surface contribution. This idea is in agreement with previous behavior found elsewhere (Furuya *et al*., 1996; Ocampo-Pérez *et al*., 2010), as will be discussed later.

It should be stressed that, in the present work, three different geometrical models of the microstructure were used (see Figure 3). From the analytical results of Ochoa-Tapia *et al*. (1993) (Chang's cells) and the numerical solution of the closure problem in domains derived from SEM micrographs, the pore effective diffusivities were calculated. The values of D_p are shown in Table 1. The results for Chang cells are significantly different than those from SEM micrographs. Since the latter is a result obtained from more "realistic" representations of the microstructure of the porous medium, it is concluded that the Chang cells are not appropriate for predicting this effective transport property for the case under study. Because Chang cells assume an isotropic medium, an analysis of the transverse and longitudinal components of the effective pore diffusivity tensor in SEM micrographs is useful to clarify the mismatch of results in Table 1.

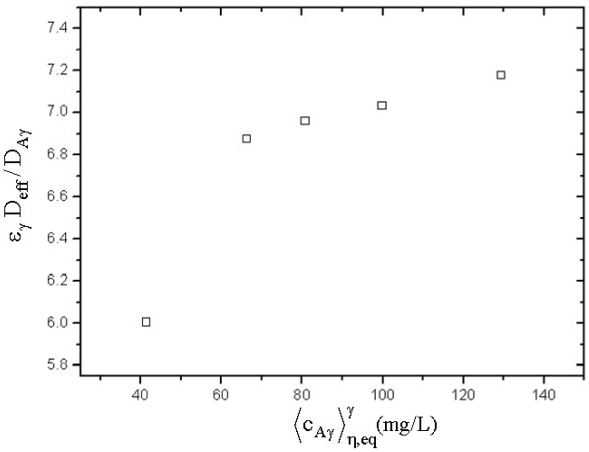

Figure 5: Effective diffusivity as function of the equilibrium concentration in the solution.

Table 1: Effective pore diffusivities for three geometrical models of the microstructure.

$\varepsilon_\gamma D_p / D_{A\gamma}$	Cylindrical cell	Spherical cell	SEM micrographs
	0.383	0.453	0.228

The value reported in Table 1 for SEM micrographs is an arithmetic average of the longitudinal and transverse diffusivity values for the three processed samples shown in Figure 6; the standard deviation of that average value is 0.02035. Additionally, in Figure 6 the xx- and yy-components of the effective pore diffusivity tensor are shown. It can be noted that the longitudinal components are larger than their transverse counterparts. This suggests that the tensor $\mathbf{D}_p$ is slightly anisotropic and suggests that the pores within the GAC are, in general, oriented in a given direction. Indeed, this anisotropy is related to the laminar microstructure experimentally observed in the GAC (Marsh and Rodriguez-Reynoso, 2006).

By subtracting the pore contribution to the effective diffusivity, the value of D_s is directly

obtained for images processed from SEM micrographs. In Table 2, the values of D_s for the three geometrical models are shown as a function of the equilibrium concentration in the solution. By comparing with the D_p values in Table 1, it can be noted that the contribution of the surface effects is larger than the pore contribution for the effective diffusivity. It leads to similar values of D_s for the analyzed geometries. In particular, a rough estimate indicates that $D_s = 12 D_{A\gamma}$.

The values of k_L for the experimental runs are reported in Table 2; this parameter ranges from 0.009 to 0.015 cm/s and has a weak and decreasing dependency with concentration. This is consistent with the trend of values reported elsewhere (Ocampo-Pérez *et al*., 2010). Finally, the fitted values of K_{eq} are also shown in Table 2. This parameter exhibits a clearly decreasing functionality with concentration and, as mentioned above, this is consistent because K_{eq} is directly related to the derivative of the nonlinear adsorption isotherm.

To conclude this work, it is opportune to take advantage of the analytical approaches given by Ochoa-Tapia *et al*. (1993) [Eqs. (16)-(19)] to calculate the local physical property D_{As}. Note that this is the only unknown parameter and it is required to find the roots satisfying Eqs. (16) and (18) in order to determine D_{As}. In Figure 7 the values of the local surface diffusivity are reported as a function of the equilibrium concentration for cylindrical and spherical Chang cells. As long as the equilibrium concentration increases, the local surface diffusivity increases. For all the cases, the results with the 3D cell are larger than those for the 2D cell. In fact, the difference between the two geometries increases with concentration.

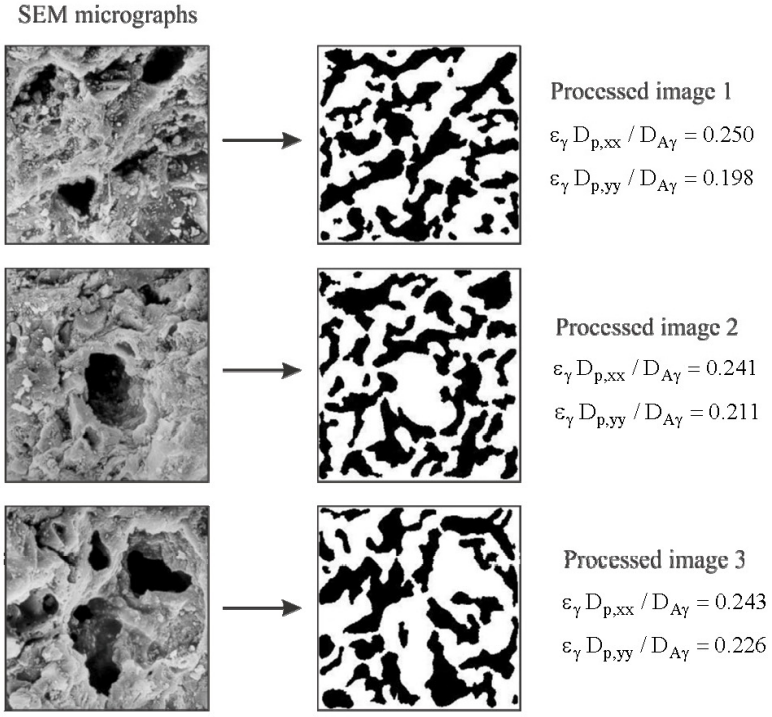

Figure 6: Longitudinal and transverse components of the effective pore diffusivity tensor for three processed images.

Table 2: Transport properties for several initial concentration of pyridine in the solution.

C_{A0} (mg/L)	$\langle c_{A\gamma} \rangle^{\gamma}_{\eta,eq}$ (mg/L)	$\varepsilon_\gamma D_s / D_{A\gamma}$			K_{eq} (cm)	k_L (cm/s)
		Cylinders	Spheres	SEM		
100	41.4	5.623	5.554	5.778	1.693×10^{-4}	0.015
200	66.3	6.493	6.423	6.648	6.872×10^{-5}	0.014
300	80.8	6.578	6.508	6.733	4.174×10^{-5}	0.013
500	99.9	6.650	6.580	6.804	2.395×10^{-5}	0.009
1000	129.4	6.793	6.724	6.948	1.228×10^{-5}	0.009

It should be stressed that the values reported in Figure 7 represent a first attempt to give a rough estimated of the local surface diffusivity. To carry this out, the simple geometries involved in the Chang cells were used. By comparison with the microstructures in the SEM micrographs in Figure 6, these are obviously poor representations of the microstructure of the GAC. However, as the effective parameter D_s was found to be weakly dependent on the local geometry, the same behavior can be inferred for D_{As}. It is recognized that this might be a serious assumption and a more detailed study must be done. Such a study would involve solving the closure problem given in Eqs. (9)-(13) in more realistic geometries like those shown in Figure 6, which in turn represents a challenging task due to the necessity of knowing the curvature H at each point in the fluid-solid matrix interface.

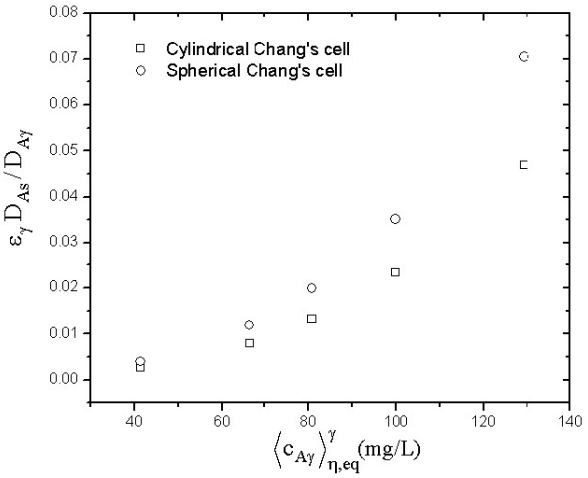

Figure 7: Local surface diffusivity as a function of the equilibrium concentration in the solution.

CONCLUSIONS

The up-scaled diffusional model given by Eqs. (23)-(28) satisfactorily interpreted the concentration decay curves of pyridine absorption onto granular activated carbon. The total effective diffusivity coefficient was found to be an increasing function of the pyridine concentration at equilibrium, mainly due to the larger contribution of the effective surface diffusion in comparison with the pore volume diffusion. In addition, a rough estimate of the point surface diffusivity was obtained by using simple geometrical models of the microstructure. In general, for the adsorption system under study, the following expression can be accepted for the different diffusivity coefficients involved:

$$D_{A\gamma} \approx 22 D_{As} \approx \frac{5}{2} D_p \approx \frac{1}{12} D_s \tag{30}$$

NOMENCLATURE

Latin Letters

$A_{\gamma\kappa}$	Geometric place of the fluid-solid interface	
a_v	Interfacial area per unit volume	m^{-1}
C_{A0}	Initial concentration of pyridine in the external fluid	kg m^{-3}
$c_{A\gamma}$	Pyridine concentration on the microscale	kg m^{-3}
$\langle c_{A\gamma}\rangle^{\gamma}_{\eta}$	Intrinsic average concentration of adsorbate in the external fluid	kg m^{-3}
$\langle c_{A\gamma}\rangle^{\gamma}_{\omega}$	Intrinsic average concentration of pyridine within the porous particle	kg m^{-3}
c_{As}	Surface pyridine concentration at the solid-fluid interface	kg m^{-2}
$D_{A\gamma}$	Molecular diffusivity of pyridine	m^2 s^{-1}
D_{As}	Molecular surface diffusivity of pyridine	m^2 s^{-1}
$\mathbf{D}_{eff}$	Total effective diffusivity tensor	m^2 s^{-1}
$\mathbf{D}_p$	Pore effective diffusivity tensor	m^2 s^{-1}
D_p	Pore effective diffusivity coefficient	m^2 s^{-1}
$D_{p,ii}$	ii-component (i = x,y) of the pore effective diffusivity tensor	m^2 s^{-1}
d_p	Average pore diameter of the granular activated carbon	m
$\mathbf{D}_s$	Surface effective diffusivity tensor	m^2 s^{-1}
$\mathbf{f}$	Closure vector	m
H	Mean curvature radius of the $\gamma-\kappa$ interface	m^{-1}
$\mathbf{I}$	Identity tensor	
K_{eq}	Adsorption equilibrium	m

	constant	
k_L	Mass transfer coefficient	m s^{-1}
m	Mass of granular activated carbon	kg
n	Number of discrete data for each experiment	
$\mathbf{n}_{\gamma\kappa}$	Unit normal vector pointing from the fluid-phase to the solid-phase	
$\mathbf{n}_{\omega\eta}$	Unit normal vector pointing from the ω- to the η-region	
R_p	Radius of the porous particles	m
S	Contact area per mass of adsorbent between the porous particle and the external fluid	m^2 kg^{-1}
S_V	Surface area per unit adsorbent mass	m^2 kg^{-1}
V	Volume of the external fluid	m^3
V_γ	Portion of the averaging volume occupied by the fluid-phase,	m^3
V_p	Pore volume per unit mass of adsorbent	m^3 kg^{-1}
$\mathbf{x}_{\omega\eta}$	Vector locating the boundary between the porous particles and the external fluid,	m

Greek Letters

ε_γ	Porosity	
ε_p	Void fraction of the particles of adsorbent	
ρ_p	Porous particle density	kg m^{-3}
ρ_s	Matrix solid density	kg m^{-3}

Subscripts

γ	Fluid phase
η	Domain of the homogeneous fluid outside the particles of adsorbent
κ	Solid matrix
ω	Domain of the particles of adsorbent

REFERENCES

Andreozzi, R., Insola, A., Caprio, V. and D'Amore, M. G., Ozonation of pyridine in aqueous solution: echanistic and kinetic aspects. Water Research, 25, 655-659 (1991).

Borges de Silva, E. A., Souza, D. P., Ulson de Souza, A. A. and Guelli U. de Souza, S. M. A., Prediction of effective diffusivity tensors for bulk diffusion with chemical reactions in porous media, Brazilian Journal of Chemical Engineering, 24, (1), 47-60 (2007).

Chang, H. C., Effective diffusion and conduction in two-phase media: a unified approach. AIChE Journal, 29, 846-853 (1983).

Currie, J. A., Gaseous diffusion in porous media: Non-steady state method. British Journal of Applied Physics, 11, 314-320 (1960).

Furuya, E. G., Chang, H. T., Miura, Y., Yokomura, H., Tajima, S., Yamashita, S. and Noll, K. E., Intraparticle mass transport mechanism in activated carbon adsorption of phenols. Journal of Environmental Engineering, 122, 909-916 (1996).

Guelli Ulson de Souza, S. M. A., Pacheco de Souza, D., Borges de Silva, E. A. and Ulson de Souza, A. A., Modelling of the dyeing process of packed cotton threads using reactive dyes. Transport in Porous Media, 68, 341-363 (2007).

Lataye, D. H., Mishra, I. M. and Mall, I. D., Pyridine sorption from aqueous solution by rice husk ash (RHA) and granular activated carbon (GAC): Parametric, kinetic, equilibrium and thermodynamic aspects. Journal of Hazardous Materials, 154, 858-870 (2008).

Leyva-Ramos, R. and Geankoplis, C. J, Diffusion in liquid-filled pores of activated carbon. I. Pore volume diffusion. Canadian Journal of Chemical Engineering, 72, 262-271 (1994).

Liu, G., Ma, J., Li, X. and Qin, Q., Adsorption of bisphenol A from aqueous solution onto activated carbons with different modification treatments. Journal of Hazardous Materials, 164, 1275-1280 (2009).

Lux, J., Ahmadi, A., Gobbé, C. and Delisée, C., Macroscopic thermal properties of real fibrous materials: Volume averaging method and 3D image analysis. International Journal of Heat and Mass Transfer, 49, 1958-1973 (2006).

Marsh, H. and Rodriguez-Reynoso, F., Activated carbon, 1st Ed. Elsevier, (2006).

Mathur, A. K., Majumder, C.B., Chatterjee, S. and Roy, P., Biodegradation of pyridine by the new bacterial isolates *S. putrefaciens* and *B. sphaericus*. Journal of Hazardous Materials, 157, 335-343 (2008).

Mohan, D., Singh, K. P., Sinha, S. and Gosh, D., Removal of pyridine from aqueous solution using low cost activated carbons derived from

agricultural waste materials. Carbon, 42, 2409-2421 (2004).

Moreno-Castilla, C., Rivera-Utrilla, J., López-Ramón, M. V. and Carrasco-Marín, F., Adsorption of some substituted phenols on activated carbons from a bituminous coal. Carbon, 33, 845-851 (1995).

Nozad, I., Carbonell, R. G. and Whitaker, S., Heat conduction in multiphase systems I. Theory and experiment for two-phase systems. Chemical Engineering Science, 40, 843-855 (1985).

Ocampo-Pérez, R., Leyva-Ramos, R., Alonso-Davila, P., Rivera-Utrilla, J. and Sanchez-Polo, M., Modeling adsorption rate of pyridine onto granular activated carbon. Chemical Engineering Journal, 165, 133-141 (2010).

Ochoa-Tapia, J. A., del Rio, J. A. and Whitaker, S., Bulk and surface diffusion in porous media: an application of the surface-averaging theorem. Chemical Engineering Science, 48, 2061-2082 (1993).

Qiao, L. and Wang, J., Microbial degradation of pyridine by *Paracoccus* sp. isolated from contaminated soil. Journal of Hazardous Materials, 176, 220-225 (2010).

Ryan, D., Carbonell, R. G. and Whitaker, S., A theory of diffusion and reaction in porous media. AIChE Symposium, 71, 46-62 (1981).

Sabah, E. and Celik, M. S., Interaction of pyridine derivatives with sepiolite. Journal of Colloid and Interface Science, 251, 33-38 (2002).

Slattery, J. C., Interfacial Transport Phenomena. Ed. Springer, New York, (1990).

Suzuki, M. and Fujii, T., Concentration dependence of surface diffusion coefficient of propionic acid in activated carbon particles. AIChE Journal, 28, 380-385 (1982).

Valdés-Parada, F. J., Alvarez-Ramírez, J., Goyeau, B. and Ochoa-Tapia, J. A., Jump condition for diffusive and convective mass transfer between a porous medium and a fluid involving adsorption and chemical reaction. Transport in Porous Media, 78, 459-476 (2009).

Valdés-Parada, F. J. and Alvarez-Ramírez, J., On the effective diffusivity under chemical reaction in porous media. Chemical Engineering Science, 65, 4100-4104 (2010).

Valdés-Parada, F. J., Aguilar-Madera, C. G. and Alvarez-Ramírez, J., On diffusion, dispersion and reaction in porous media, Chemical Engineering Science, 66, 2177-2190 (2011).

Whitaker, S., The Method of Volume Averaging. Kluwer Academic Publishers, Netherlands, (1999).

Zhang, C. and Wang, Y., Removal of dissolved organic matter and phthalic acid esters from landfill Leachate through a complexation–flocculation process. Waste Management, 29, 110-116 (2009).